

FULL ARTICLE

Phagocytosis and immune response studies of Macrophage-Nanodiamond Interactions *in vitro* and *in vivo*

K.-J. Huang^{1,4}, C.-Y. Lee², Y.-C. Lin², C.-Y. Lin¹, E. Perevedentseva^{2,3}, S.-F. Hung¹, and C.-L. Cheng^{*,2}

¹ Department of Life Sciences, National Dong Hwa University, 1, Sec. 2 Da Hsueh Rd, Shoufeng, Hualien, 97401, Taiwan

² Department of Physics, National Dong Hwa University, 1, Sec. 2 Da Hsueh Rd, Shoufeng, Hualien, 97401, Taiwan

³ P.N. Lebedev Physics Institute, Moscow 119991, Russia

⁴ Institute of Biologicals, Development Center for Biotechnology (DCB), New Taipei City, 22180, Taiwan

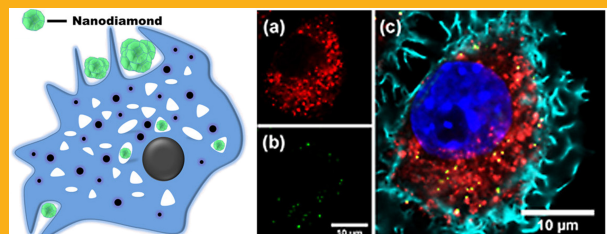
Received 14 July 2016, revised 31 October 2016, accepted 22 November 2016

Published online 10 January 2017

Key words: nanodiamond, macrophage, immunological response, cytotoxicity, bio-labeling

The applications of nanodiamond as drug delivery and bio-imaging can require the relinquishing ND-drug conjugate via blood flow, where interaction with immune cells may occur. In this work, we investigated the ND penetration in macrophage and the immune response using the tissue-resident murine macrophages (RAW 264.7). Confocal fluorescence imaging, immunofluorescence analysis of nuclear translocation of interferon regulatory factor IRF-3 and transcriptional factor NF- κ B, analysis of pro-inflammatory cytokines production IL-1 β , IL-6 IL-10 with a reverse transcription-polymerase chain reaction technique were applied. The TNF- α factor production has been studied both *in vitro* at ND interaction with the macrophage and *in vivo* after ND injection in the mice blood system using immunoassay. The macrophage antibacterial function was estimated through *E. coli* bacterial colony formation. ND didn't stimulate the immune response and functionality of the macrophage was not altered. Using MTT

test, ND was found negligibly cytotoxic to macrophages. Thus, ND can serve as a biocompatible platform for biomedical applications.



Left: Graphic representation of Nanodiamond internalization in macrophage. Right: (a) Fluorescence images of lysosomes, (b) nanodiamond and (c) merged image of nanodiamond internalization in macrophage.

1. Introduction

Recent development in nanobiotechnology opens new facilities for bio/medical applications using nanostructured materials. This offers new perspectives in medical practices, but also raises questions termed as nanosafety. Using nanoparticles for targeted drug

delivery allows increasing the efficiency of treatment [1, 2]; such applications usually require delivery of nanoparticle-drug composites to the targets via the blood flow, where contact of the nanoparticle with the immune system can be expected. When immune cells in the blood (monocytes, leukocytes, dendritic cells, etc.) and in tissues (resident phagocytes,

* Corresponding author: e-mail: clcheng@mail.ndhu.edu.tw, Phone: 886-3-8632021

macrophages) engulf and eliminate the nanoparticles, their interaction is determined by both cell type and particle properties.

When nanoparticles interact with the cells of immune system, it can cause immune responses such as immunostimulation (inflammation, including the specific cytokines production, generation of nanoparticles-specific antibodies) or immunosuppression which could reduce the resistance of organism towards infections and cancerous cells [3]. The activity of immune cells can also reduce the number of nanoparticles available to reach the target [4]. The study of the nanoparticles effect on immune cells is a subject of serious research interest, particularly the effect on macrophage whose functions are to remove foreign materials by ingesting them through phagocytosis and stimulating other immune cells [5]. The mechanisms of engulfment of different nanoparticles by macrophage and immune response stimulation [6] have been studied, including amorphous silica [7, 8], silver [9, 10], gold [11], polymers [12, 13], etc., however their effect on macrophage is not clearly understood, even for the clinically used nanoparticle, e.g. ferucarbotran (superparamagnetic iron oxide), magnetic resonance imaging contrast agent [14].

Nanodiamond (ND) has emerged to be a platform for various bio-medical applications owing to its biocompatibility [15–17] and remarkable physical-chemical properties; particularly its spectroscopic properties can be used for bio labeling [17–22]. Taking advantage of ND's surface properties, various methods for biomolecule/drug immobilization on ND [23–25] are suggested and successful cell internalization, drug and gene delivery have been demonstrated [17, 25–27]. With the increasing interest placed on nanodiamond for its promising bio-medical *in vivo* applications, the issue of immunological response gains the prior importance.

Earliest *in vivo* researches [38] demonstrated the effect of ND obtained by detonation method (DND) on the cells of immune system consisting in increased levels of blood leucocytes accompanied by changes in some biochemical parameters of the animals' blood plasma at perioral administration and injections. *In vitro* ND-blood interaction showed no destruction of blood cells, including leucocytes and erythrocytes [39], as well as no increased inflammatory cytokines [40]. Later, the increase in the total level of white blood cells in mice has been observed as result of peroral receiving DND and is explained as a consequence of the interaction between DND and gastrointestinal macrophages [41]. Additionally, ND can affect the process of generating reactive oxygen species (ROS) which is an important element of innate immune system stimulation and inflammation processes [39, 42]. The effect of DND on phagocytic activity and oxidative burst of innate immune cells has been studied *in vivo* on rat model [42]; both

intravenous and intraperitoneal administration of ND hydrocolloid has decreased the number of phagocytosing neutrophiles stimulated by *E. coli* and increased the number of cells with stimulated oxygen-dependent bacteria elimination. Also, the works analyzing DND interaction with immune cell conclude that DND in dose-dependent manner modifies the activity of phagocytes which can be useful in regulating treatment of inflamed sites [43]; the ND effects on the macrophage responses by analyses of cell proliferation, cell viability and cell morphology, apoptosis and phagocytosis, and genetic expression of pro-inflammatory cytokines and chemokines were also observed. In a study of the inflammatory effect of nanodiamond wear debris particles on macrophage, the smaller the size of ND and the higher the concentrations, the more pronounced the damage have been found [44, 45]; but no inflammation has been observed due to diamond particles treatments at low concentrations.

In present work, we study the interaction of ND of nominal size 100 nm with the tissue-resident murine macrophages, RAW 264.7, as the cellular model. The properties of ND (crystal structure, surface, aggregation) vary significantly with its sizes. In this work we study relatively large ND (100 nm ND), obtained with method of High Temperature/High Pressure (HTHP), giving ND with good diamond structure and low contents of surface graphite, and these ND are already found as more bio-compatible in comparison with ND obtained by detonation (with smaller size of crystallites, but high content of graphite and stronger aggregation).

The cytotoxicity of ND for macrophages is analysed using MTT assay. The mechanism of ND engulfment by macrophage is analyzed via blocking different possible pathways. The macrophage immune reactions including pro-inflammatory cytokine expression and immune-associated transcriptional factors (IRF-3, NF- κ B) activation are studied with the reverse transcription-polymerase chain reaction (RT-PCR) technique and the immunofluorescence analysis. The TNF- α production stimulated by ND is studied *in vitro* at interaction with the RAW 264.7 cells and *in vivo* on animal (mice) model after ND injection in the blood system. It is found ND neither induces macrophage to produce the pro-inflammatory cytokines nor activate those correspondent transcriptional factors which doesn't disturb the macrophage functionality. ND is found non-cytotoxic to macrophages and is engulfed by macrophages through the clathrin-mediated endocytosis pathway, with ND entrapping by lysosomes in the cytoplasm. The functionality of the macrophage at interaction with ND is estimated using bacterial colony formation. The effects of macrophage and macrophage treated with ND on *E. coli* surviving and division are comparable.

2. Materials and methods

2.1 Nanodiamond

Nanodiamond of nominal size 100 nm produced with high temperature/high pressure method (HTHP) is used (Kay Diamond, USA); usually referred as 100 nm ND. The measured average size of ND used in this experiment is 130 ± 25 nm with variable shapes and surfaces. The size should be measured in every concrete case, because ND size distribution depends not only on size of the crystals but on aggregation, which depends both on ND properties and medium for ND suspension and ND concentration. Both the as-received ND and the carboxylated nanodiamond (cND) are used. For carboxylation, ND has been subjected to strong acid (H_2SO_4 : $\text{HNO}_3 = 3:1$) treatment which removes the impurities and disordered carbons on the surface [46]. The ND has been suspended in cell growth mediums with concentrations of 1–100 $\mu\text{g}/\text{ml}$. The ζ -potential, size and aggregation of carboxylated ND have been analyzed using the Zetasizer Nano ZS (Malvern Instruments, UK). The ζ -potential was evaluated to be about -40 mV at physiological pH (7.2–7.4).

2.2 Cell culture and imaging

Murine leukaemic monocyte macrophage cells RAW 264.7 were cultured in a flask at 37°C and 5% CO_2 in a humidified incubator (310/Thermo, Forma Scientific, USA) in Dulbecco's Modified Eagle's Medium (DMEM, Biowest, USA) with 2 mM L-glutamine (Invitrogen, USA) containing 5% FBS (Invitrogen, US), 1 mM Sodium pyruvate (Invitrogen, USA) and 10 $\mu\text{g}/\text{ml}$ polymyxin B (Calbiochem, USA), to prevent bacterial contamination in cell culture. Cultured cells were kept overnight in 60 mm Petri dish with glass coverslip placed at the dish bottom.

To activate the macrophage, 0.1 $\mu\text{g}/\text{ml}$ lipopolysaccharides (LPS) from outer membrane of Gram-negative bacteria (Sigma, USA), or 40 $\mu\text{g}/\text{ml}$ poly (I:C) (synthetic double strand RNA, consists of I:C sequences, Calbiochem, USA) were added and kept undisturbed overnight. The inactivated and activated cells were further treated with ND. ND was added to the medium with the concentrations ranging from 1–100 $\mu\text{g}/\text{ml}$ and cells were incubated together with ND for 30–240 min. Unreacted ND was removed by washing. The samples of cells with NDs adhered on the coverslips were used for microscopic investigations.

A laser confocal microscope (TCS SP5, Leica, Germany) equipped with UV laser (405 nm), argon

laser (458/476/488/514 nm) and HeNe laser (543 nm/633 nm) was employed for fluorescence studies of ND interactions with macrophages, ND penetration into the cell at alternatively blocking pathways, and for immunofluorescence analysis. In general, the color centers/defects induced fluorescence of ND can be excited with various wavelength lasers, and with emission between 500–800 nm. We used different excitation lasers and emission was collected at different ranges to avoid overlapping/confusion with the molecular dyes used to dye the cells.

To observe the interaction of ND with macrophages, the activated and inactivated cells with ND adhered on glass substrate were fixed with 3.7% formaldehyde in PBS for 10 min and then were permeabilized with 0.01% TritonX-100 in PBS for 10 min. After several washings with PBS, the samples were blocked with 1% BSA and the RNA was removed by incubating with 200 $\mu\text{g}/\text{ml}$ RNase in PBS for 20 min. The f-actin of cytoskeleton was stained with 20 μM Alexa 647-conjugated Phalloidin (Invitrogen, USA) for 20 min and the nuclei were stained with 5 mM Sytox Green (Invitrogen, US) for 3 min. The samples were three-times washed with 0.01% Triton X-100 in PBS. All prepared samples were mounted with Vectashield mounting medium (Vector Laboratories, USA) and stored in the dark at 4°C before analysis. For the ND distribution analysis using laser confocal microscope the cell nuclei dyed with Sytox Green were excited with 488 nm laser and the emission was collected in the wavelength range of 505–568 nm. F-actin stained with Phalloidin-Alexa 647 was excited by 633 nm laser, and the emission was collected in the range of 646–725 nm. ND fluorescence was excited by 488 nm wavelength laser and its emission was detected in the 590–625 nm wavelength range.

To observe the interaction of ND and cell in real-time, the differential interference contrast (DIC) imaging was used. Cells were incubated with 10 $\mu\text{g}/\text{ml}$ ND, placed in a cell culture chamber and examined by confocal microscopy at an interval of 3 min simultaneously for acquiring the ND fluorescence images and the DIC optical images. The 100 nm ND was excited by 633 nm wavelength laser, and its emission was recorded in the 648–764 nm wavelength range.

2.3 Cytotoxicity analyses with MTT Assay

To estimate *in vitro* nanodiamond cytotoxicity, the RAW 264.7 cell viability was tested with MTT assay. Cells were seeded (4×10^5 cells/well) in a 96-well microtitre plate in DMEM, supplemented with 2 mM L-glutamine (Invitrogen, USA) containing 5% fetal bovine serum (FBS) and incubated at 37°C and 5%

CO₂ for 24 hours. After incubation, the medium was aspirated. The cells activated with LPS (0.1 µg/ml) and inactivated cells were treated with fresh medium containing different concentrations (6.25–100 µg/ml) of ND for 24 h and 6 h. After the incubation, the medium was removed and the cells were treated for 3 h with MTT reagent (the concentration was 2.5 mg/ml), then the solution was removed and 200 µl dimethyl sulfoxide (DMSO) was added to dissolve formozan. ELISA reader (MRX revelation Microplate Reader, DYNEX, USA) was used to measure the optical absorption at 570 nm (O.D.₅₇₀ value). Relative percentages of surviving cells were calculated by dividing the absorbance of treated cells with that of control in each experiment.

2.4 ND uptake mechanism and its cellular distribution

To analyze the ND uptake mechanisms, different possible engulfment pathways were selectively blocked. To block energy-dependent processes, cells were pre-incubated at 4 °C in PBS for 30 min or in PBS containing 10 mM sodium azide NaN₃ (Sigma, USA) for 30 min at 37 °C. To block phagocytosis, cells were treated with cytochalasin D (Enzo Life Sciences, USA). Cells were incubated in PBS supplied with 10 µg/ml of cytochalasin D for 30 min. The clathrin-independent (caveolae) pathway was blocked by filipin (Filipin III from Streptomyces filipinensis, Sigma, USA). The cells were pre-incubated with PBS buffer supplemented with 5 µg/ml filipin for 30 min at 37 °C. To block clathrin-dependent endocytosis, the cells were pre-incubated with PBS supplemented with 10 M chlorpromazine (Enzo Life Sciences, USA) for 30 min at 37 °C or subjected to hypertonic treatment with 0.45 M sucrose in PBS for 30 min at 37 °C. After treatment the cells were washed and incubated with 20 µg/ml ND in DMEM medium for 4 h at 37 °C. These cells were fixed and dyed for imaging, the cell nuclei were stained with 1 µg/ml DAPI (Invitrogen, USA) and the cytoskeletons were stained with the Phalloidin-Alexa 647 (Invitrogen, USA).

To trace the cellular distribution of ND, macrophages were incubated with 100 nm ND (2 µg/ml in medium) for 6 h, and then fixed for organelle staining: lysosomes were dyed using 50 nM Lysotracker Red DND-99 (Invitrogen, USA) for 1 h, the nuclei and cytoskeleton were dyed with DAPI and Phalloidin-Alexa 647 as described above. The emission of Lysotracker was detected at 590 nm.

2.5 ND effect on the activation of the immunological regulators

To evaluate the activation of the immunological regulators in macrophages after ND treatment the nuclear translocation of IRF-3 or NF-κB factors was assayed by the immunofluorescence assay. RAW 264.7 cells (2×10^5 cells/dish) were cultured overnight with the medium supplemented by 10 µg/ml polymyxin B (Calbiochem, USA) on a pre-embedded sterile glass coverslip at the bottom of the 60 mm Petri dish. The cells were treated with 100 nm ND at various concentrations of 20, 50, 100 µg/ml for 24 h and then were subjected to immunofluorescence assay. Cells were incubated with primary anti-IRF-3 (GeneTex, USA) or anti-NF-κB p105/p50 antibodies (GeneTex, USA) and then washed with PBS before staining with the anti-Rabbit Hilyte Fluor™ 488-labeled secondary antibodies (AnaSpec, USA). The stained cells were counterstained as the cellular nuclei and cytoskeleton were dyed with DAPI and Phalloidin-Alexa 647, respectively. The LPS (0.1 µg/ml) or poly (I:C) (40 µg/ml) were used as the positive controls to stimulate the nuclear translocation of IRF-3 or NF-κB.

The action of NF-κB on gene expression in ND-treated cells was conducted in RAW-Blue cells (Invitrogen, USA) where a secreted embryonic alkaline phosphatase (SEAP) gene was engineered under a promoter control by NF-κB and AP-1 transcription factors. RAW-Blue cells were plated (4×10^5 /well) into a 96-well plate with medium supplemented with 5% heat-inactivated fetal bovine serum (Invitrogen, USA), 2 mM L-glutamine (Invitrogen, USA) and 100 µg/ml Normocin (Invitrogen, USA), and then incubated overnight before treatment with different concentration (25 µg/ml and 100 µg/ml) of 100 nm NDs or cNDs for another 24 hours. The LPS (0.1 µg/ml) was used as a positive control. The harvested cell culture supernatant (40 µl) was mixed with 160 µl working QUANTI-Blue substrate (Invitrogen, USA) and incubated at 37 °C for 30 min to 6 h prior measure at O.D.₆₂₀ by a EnSpire spectrophotometer (PerkinElmer, USA).

2.6 Measurements of TNF-α in vitro and in vivo production

For the *in vitro* test the RAW 264.7 cells were seeded in a 6-well plate (1×10^6 /well) and treated with 100 nm ND or cND at various concentrations of 25 µg/ml, 50 µg/ml, 100 µg/ml for 24 h and LPS in concentration of 0.3 µg/ml as a positive control. After treatment, the cell culture supernatants was taken and stored at -80 °C until measurements.

For animal test, 8 weeks-old male C57BL/6 mice ($n = 6$) weight 22–24 grams were used. The mice were purchased from the National Laboratory Animal Center and housed in the Laboratory Animal Center, Tzu-Chi University (Hualien Taiwan), until they were 8–9 weeks old. The mice underwent the procedures under anesthesia with an intraperitoneal injection of ketamine: xylazine (80: 10 mg/kg body weight). The research methods were approved by the Animal Care and Use Committee of National Dong Hwa University (approval ID100004).

The NDs suspended in concentration 1 mg/ml in PBS and sonicated for 3 min were injected to mice via the caudal vein (c.v.) route in quantity 20 mg/kg of body weight (b.w.) or LPS in concentration 1000 ng/kg of b.w. The animals of the control group have received the same volume (20 μ l per 1 gram of b.w) of PBS solution. Blood samples were collected via orbital sinus of the mice at 2 and 6 h after injection. The collected blood samples were immediately placed on ice and within 10 min the plasma was separated by centrifugation at 400 g for 10 min and aliquoted for storage at -80°C until measurements. Cell culture supernatants and mice blood serums were assayed for TNF- α levels by AlphaLISA Mouse Tumor Necrosis Factor alpha (mTNF- α) kit (Blossom biotechnologies Inc., Taiwan), details see Suppl. Mater. (1) [47].

2.7 Detection of proinflammatory cytokines by reverse transcriptase polymerase chain reaction (RT-PCR)

The RAW 264.7 cells were plated (1×10^6 /well) in a 6-well plate with DMEM supplemented with 5% heat-inactivated FBS (Gibco, USA), 2 mM L-glutamine (Gibco, USA) and then cultured overnight. Cells were treated with 25 μ g/ml of 100 nm NDs or cNDs in the presence of 10 μ g/ml of polymycin B, or 0.1 μ g/ml LPS for 6 and 24 hours. After incubation, total cells were harvested and 1 μ g RNA extracted by RNeasy mini kit (Qiagen, Germany) was reverse transcribed into complementary DNA (cDNA) by using oligo (dT) 18 primer and Moloney Murine Leukemia Virus Reverse Transcriptase (M-MLV RT) (Invitrogen, USA). The specific cytokine message RNA (mRNA) was amplified by polymerase chain reaction (PCR) with specific paired-primers in 2 \times PCR master mix solution (i-Taq) (iNtRON biotechnology). IL-1 β , IL-6, IL-10, TNF- α , β -actin primer sequences [48], (see in Suppl. Mater. (2)). PCR was carried out with the ABI Veriti (PE Applied Biosystems, USA). The PCR conditions were: 95 °C for 2 min, 25 cycles of 95 °C for 30 s, 50–58 °C for 40 s, and 72 °C for 40 s. The resultant amplified

DNA fragments were resolved in 2% agarose gel, stained with 0.5 μ g/ml ethidium bromide (EtBr) and then visualized by Dolphin-view gel imager (Wealtec, USA).

2.8 ND effect on macrophage's bactericidal activity

The effect of ND on macrophage's bactericidal activity was evaluated using bacterial colony formation test. RAW 264.7 cells were cultured with DMEM supplemented with 5% FBS and 2 mM L-glutamine in the 12-well plates (2×10^5 cells/well), and then incubated at 37°C and 5% CO_2 overnight. The cells were treated with or without 20 μ g/ml of 100 nm ND in medium for 24 hours and the un-reacted NDs were removed from cells by washing three times with PBS (pH \sim 7.4). Then, the cell culture was co-incubated with bacteria *E. coli* suspension (O.D.₆₀₀ = 0.9) for 4 hours. The culture supernatant was harvested; 10-fold serially diluted with PBS, and spread out on Luria-Bertani (LB) agar plate. The numbers of bacterial colonies in each plate were counted after 12-hour incubation and were reversely correlated to the macrophage's bactericidal function.

2.9 Statistical analysis

The experimental results were presented as mean \pm standard deviation (SD). Statistical difference between two groups was made using two-tailed Student's *t*-test. The *P*-value of <0.05 was considered statistically significant.

3. Results and discussion

3.1 Internalization of nanodiamond

Optical and laser confocal imaging was used to observe the interaction of macrophage with 100 nm ND. The engulfment of ND by the RAW 246.7 cell was imaged *in situ*, and results are shown in Figure 1. In Figure 1(I), pseudopodia protruding the cell, wrapping up the ND and then internalizing it into cytoplasm with the morphological transformation during the engulfment process (18 min) is observed. The location of ND inside the cell was evidenced by the *z*-scanning (Figure 1(II)), and ND has been found co-localized with lysosomes after 6 h of the incubation (Figure 1(III)). We did not observe the expelling ND from cells within 48 h of observation.

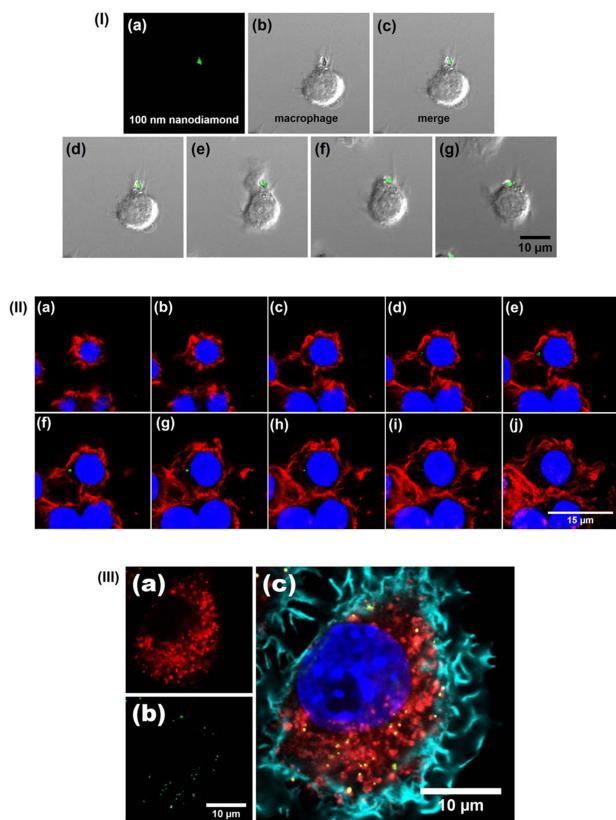


Figure 1 Internalization of ND. (I) Interaction of RAW 264.7 cell with 100 nm nanodiamond (concentration 10 $\mu\text{g}/\text{ml}$). (a) The fluorescence image of a single 100 nm nanodiamond at excitation 633 nm; (b) DIC image of the macrophage; (c) merging (a) and (b); (d–g) merged DIC and fluorescence images during the engulfing process of ND by macrophage, consequently measured every 3 min. (II) The confocal fluorescence images of RAW 264.7 with ND (concentration 1 $\mu\text{g}/\text{ml}$) scanned along z -axis with 340 nm step. Cell nuclei dyed with Sytox Green (shown in blue); cytoskeleton stained with Phalloidin-Alexa 647 (red); ND fluorescence excited at 488 (green). (III) Trafficking of nanodiamond inside the macrophage RAW 264.7 co-cultured with 100 nm ND (25 $\mu\text{g}/\text{ml}$) for 6 h. (a) Lysosomes stained by Lysotracker-Red; (b) nanodiamond fluorescence excited with 488 nm (green); (c) merged image, cell nuclei dyed with DAPI (blue); cytoskeleton stained with Phalloidin-Alexa 647 (cyan).

Since ND is entrapped in lysosomes, the interaction of ND with intracellular structures can be limited.

3.2 Uptake and toxicity of ND for a macrophage

Macrophages activated by LPS are more potent to engulf substances, e.g. bacteria. The uptake of 100 nm NDs by activated and non-activated macro-

phage RAW 246.7 cells, at various time of joint incubation and at various concentrations are compared. The percentage of cells engulfing the ND was estimated using confocal imaging (Figure 2). The histogram in Figure 2(I) shows that for low ND concentration (10 $\mu\text{g}/\text{ml}$), the number of non-activated cells engulfing ND increases from ~1% to ~4% at increasing incubation time from 30 to 240 min. For the activated cells, the uptake increases more significantly with increasing incubation time and number of cells containing ND can reach ~7%. In general, the uptake depends linearly on the time in the observed time interval. MTT test was used to estimate survival rate of the macrophage and LPS-activated macrophage treated with ND with various concentrations (6.25–100 $\mu\text{g}/\text{ml}$) and incubation time (Figure 2(II)). Results show that at 6 h of joint incubation more than 90% of both activated and inactivated cells survive. At 24 h, this surviving rate remains high and consists of more 80% of the cells. This concludes that 100 nm ND is not cytotoxic for RAW 246.7 macrophage like in most of previous cells studies [15–21].

3.3 ND internalization pathways

The possible internalization pathways are schematically drawn in the Figure 3(I). To investigate the pathways of ND internalization by macrophage, different possible pathways were selectively blocked, and the resulting histogram is shown in Figure 3(II), where the relative numbers of ND-internalizing cells after corresponding blocking treatments are plotted. Normal culture condition was used for control cell culturing. To evaluate the contribution of energy-dependent uptake, the endocytosis was suppressed by low temperature (incubation at 4 °C), or cells were transferred to dormant state being inactivated by the ATP depletion via treatment with 10 mM of NaN_3 . Significant decrease in the internalization (Figure 3(II)) at these conditions suggests that energy-dependent endocytosis pathway dominates for ND penetration into the macrophage. To analyze the contributions of different energy-dependent pathways, cytochalasin D (10 $\mu\text{g}/\text{ml}$) was used to block the phagocytosis pathway. A high level of internalization reveals the receptor-mediated endocytosis pathway. When treatment with 0.45 mM sucrose blocks the clathrin-mediated process, a significant decrease in the uptake confirms the clathrin-dependent pathway. This was confirmed by blocking the clathrin-independent pathway with 5 mg/ml filipin without the uptake decreasing. Thus, clathrin-dependent endocytosis is the main pathway for ND penetration in macrophage cell. This result is similar to previous studies on ND penetration into different kinds of

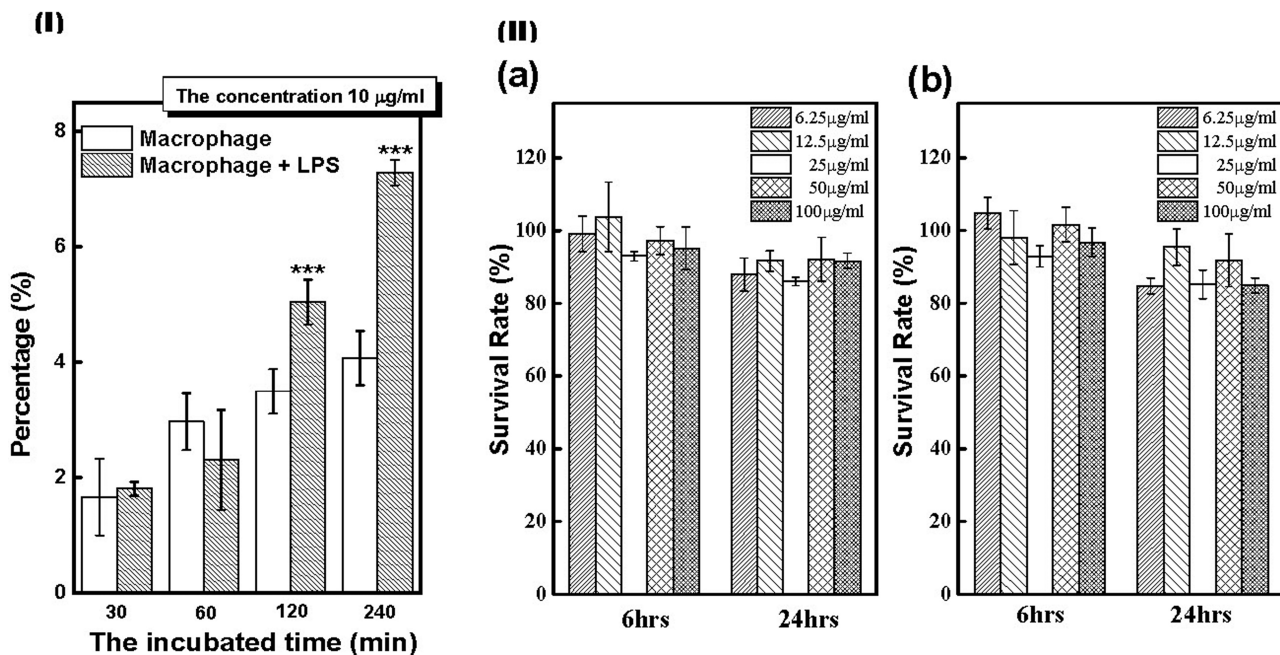


Figure 2 (I) Time-dependent uptake of 100 nm ND by RAW 264.7 cells, non-activated and activated with LPS (0.1 µg/ml) and ND (10 µg/ml). $n = 3$, *** $P < 0.001$. Data are mean \pm SD; (II) Cytotoxicity test: the surviving rate of macrophage treated with 100 nm ND of various concentrations: (a) non-activated cell; (b) the cell activated by LPS. $N = 3$, ns, $P > 0.05$ was considered not significant. Data are mean \pm SD.

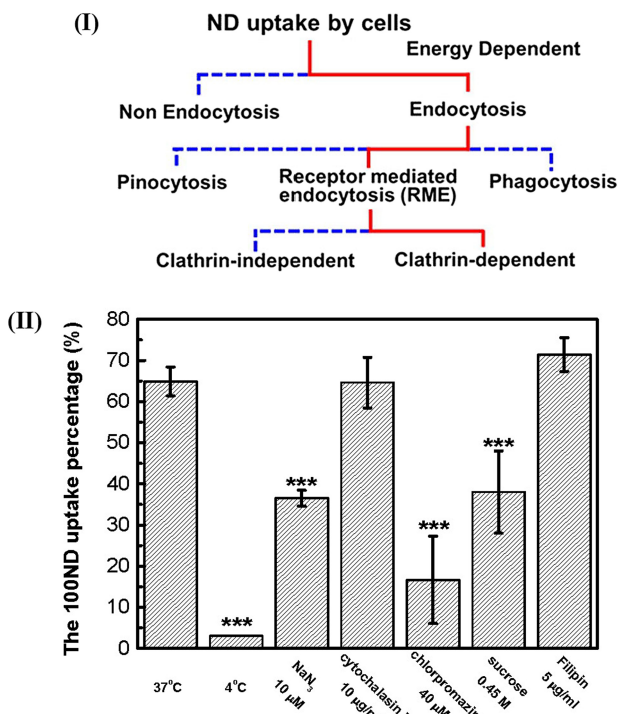


Figure 3 (I) Scheme for possible ND internalization pathways in macrophage; (II) 100 nm ND (concentration 20 µg/ml) engulfment by non-activated RAW 264.7 at blocking different pathways. $N = 3$, *** $P < 0.001$, significantly better as compared with 37 °C control groups. Data are mean \pm SD.

cells [21, 31–35], including our studies comparing cancer and non-cancer cells [35].

3.4 The effect of NDs on macrophage's activities

When macrophages sense intruding substance (e.g. microbes) they synthesize and release the proinflammatory cytokines and chemokines to activate and recruit other immune cells to expel the invading substance. Binding of the dangerous ligands such as viral RNA (dsRNA) or LPS to their corresponding pattern recognition receptors such as Toll-like receptors TLR3 and TLR4, respectively, on macrophages' cell surface initiates the intracellular signaling cascade to activate certain transcriptional factors e.g. IRF-3 and NF- κ B, resulting in the expression of the interferons; proinflammatory cytokines and chemokines. Upon activation, IRF-3 is phosphorylated and translocate from cytoplasm to nucleus to initiate interferon mRNA synthesis. NF- κ B dissociates from its pre-complex inhibitor, I- κ B, and moves from cytoplasm to nucleus to activate certain NF- κ B-regulated genes, including proinflammatory cytokines and chemokines [48]. Treatment of cells with 20 µg/ml ND resulted in neither IRF-3 nor NF- κ B activation as no nuclear translocation were observed for each molecule. In contrast, treatment with poly (I:C)

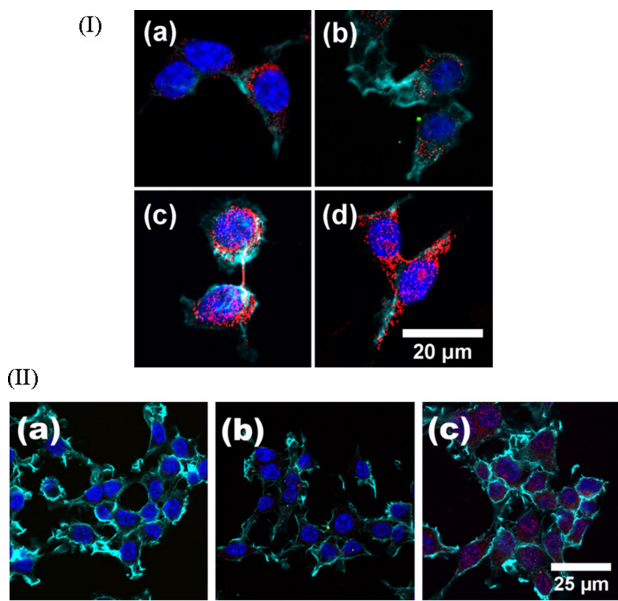


Figure 4 No activation of the immunological regulators in the RAW 264.7 macrophage by ND. **(I)** IRF3 translocation in nuclei. **(a)** Control: RAW 264.7 with nuclei labeled with DAPI (shown in blue), the cytoskeleton stained with Phalloidin (cyan), IRF3 bounded with primary antibody Anti-IRF3 and secondary Anti-Rabbit Hylite Fluor™ 488-labeled antibody (red). **(b)** RAW 264.7 treated with 100 nm ND (concentration 20 µg/ml); ND fluorescence exited with 488 nm is shown in green. **(c)** RAW 264.7 activated by LPS (concentration 0.1 µg/ml). **(d)** RAW 264.7 activated by poly(I:C) (concentration 40 µg/ml). **(II)** NF-κB translocation in nuclei. **(a)** RAW 264.7; NF-κB proteins are bounded with primary antibody Anti-NF-κB and then with the secondary Anti-Rabbit Hylite Fluor™ 488-labeled antibody (red). **(b)** RAW 264.7 treated with 100 nm ND (concentration 20 µg/ml). **(c)** RAW 264.7 activated by LPS (concentration 0.1 µg/ml).

(40 µg/ml), a synthetic dsRNA, or LPS (0.1 µg/ml) did induce the nuclear transduction of IRF-3 or NF-κB molecules (Figure 4). The ND effect on macrophages for the production of proinflammatory cytokines was evaluated by checking the corresponding mRNA levels using reverse-transcriptase polymerase chain reaction (RT-PCR) method. The mRNA expression of certain proinflammatory cytokines such as TNF-α, IL-1β and IL-6, was not detected in either ND or cND treatment (25 µg/ml). In addition, no proinflammatory cytokine production was observed due to the induction of suppressive cytokine, such as IL-10 after ND treatment (Figure 5(I)). To further confirm that ND is an immuno-compatible material, the NF-κB-responsible promoter reporter system was conducted. The RAW-Blue cells were engineered with a secreted embryonic alkaline phosphatase (SEAP) gene regulated by NF-κB and AP-1 transcription factors. Upon stimulation of the RAW-Blue cells with LPS, NF-κB is activated and translo-

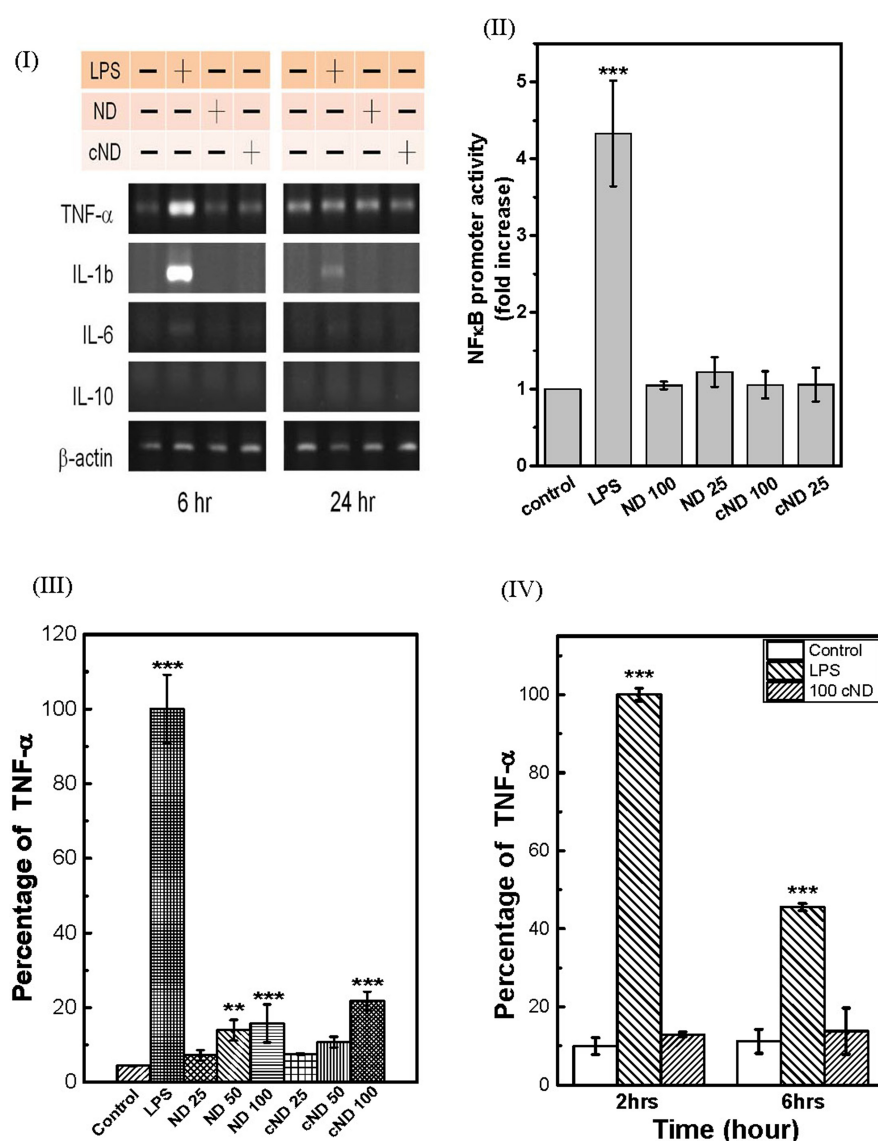
cated into nucleus, to initiate the SEAP expression. The SEAP activities proportional to the NF-κB activation were assayed by adding the QUANTI-Blue substrates. Treatment of RAW-blue cells with different concentration of NDs (25 µg/ml and 100 µg/ml) has no effect on NF-κB activation and no difference in SEAP activities between control and ND-treated groups. In contrast, RAW-blue cells treated with 0.1 µg/ml LPS induced the SEAP expression and its activity was four times higher than for control and ND-treated groups (Figure 5(II)). To confirm the results, the TNF-α production by RAW 264.7 macrophages after ND treatment with different concentration of NDs (25 µg/ml, 50 µg/ml and 100 µg/ml) was analyzed. The TNF-α production was not activated by ND in comparison with control group (treatment with PBS) while increased TNF-α level in the RAW 264.7 treated with 0.3 µg/ml LPS was observed (Figure 5(III)). In the animal test, *in vivo* ND application to mice blood system also demonstrated no activation of the TNF-α production. In the control group with LPS treatment, higher level TNF-α in blood plasma was detected (Figure 5(IV)).

3.5 The macrophage functional test

To understand, how the ND treatment can affect the macrophage immune function, the effect of the macrophage and ND-treated macrophage (with 20 µg/ml of 100 nm ND for 24 h) on bacteria *E. coli* colonies formation is compared. The numbers of *E. coli* colonies are presented in diagram (Figure 6). Results show the number of *E. coli* colonies in control did not change compared to the number of colonies after treatment with 100 nm ND (20 µg/ml; 24 h). This confirms our previous observations, that 100 nm ND is not toxic for bacteria [49]. A significant decrease in the number of the colonies was observed both in macrophage and macrophage treated with ND. Almost the same result observed with *E. coli* colonies number in the ND pre-treated macrophage's group proves that ND treatment does not suppress the immune function of the macrophages. It evidences the biocompatibility of 100 nm HTHP nanodiamond. However, previous *in vivo* study has demonstrated that the process of phagocytosis and anaerobic mechanisms of microbe elimination were significantly impaired by DND [42].

The study of the nanoparticle effect on immune cells is now the subject of serious research interest, particularly the interaction of nanoparticles with macrophages whose function is to isolate foreign materials by ingesting them through an endocytosis and to stimulate other immune cells. Number of works describes the engulfment mechanism of different kinds of nanoparticles by macrophage and immune

Figure 5 Immuno-compatibility of ND with proinflammatory cytokine production. **(I)** Expression of proinflammatory cytokines in ND-treated RAW 264.7 cells detected by RT-PCR. The cells were treated with 25 μ g/ml 100 nm ND and 0.1 μ g/ml LPS for 24 h. **(II)** Assay of NF- κ B activation in ND-treated RAW cells. RAW-Blue Cells were co-cultured with different concentrations (25 and 100 μ g/ml) of 100 nm NDs or cNDs for 24 hrs and the LPS as a positive control. $N = 3$, *** $P < 0.001$. Data are mean \pm SD. **(III)** *In vitro* test of TNF- α activation in RAW 264.7 cells treated with 100 nm ND or cND at various concentrations of 25, 50, 100 μ g/ml for 24 h and LPS in concentration of 0.3 μ g/ml as a positive control. $n = 6$ (three experiments repeated twice); ** $P < 0.01$, *** $P < 0.001$. Data are mean \pm SD. **(IV)** *In vivo* test of TNF- α activation in the blood system of mice after injection of cND (suspended in PBS with concentration 1 mg/ml) in quantity 20 mg/kg of body weight or LPS in concentration 1000 ng/kg of b.w. as a positive control. Blood samples collected at 2 and 6 h after injection. $n = 6$ (three experiments repeated twice); *** $P < 0.001$. Data are mean \pm SD.



response stimulation [6]. The engulfment pathways and immune response can differ for different cell types [12, 50–52]. Moreover the effect on immune cells is also different for nanoparticles of different nature [12, 13, 53], various sizes [10, 50], mechanical properties [54], surface charge and hydrophobicity/hydrophilicity [55]. Thus, any nanoparticle newly developed for bio applications should be analyzed in terms of its compatibility with immune system. As for nanodiamond, surface coating is one of the most important parameters of ND [56], which can determine the interaction with environment, preventing non-specific adsorption and can facilitate the interaction with specific cell. Note, that varying properties of ND, including roughness and aggregation [57] make it necessary to analyze every new-applied nanoparticle's interaction with many different kinds of cells, even if not to mention the more highly orga-

nized systems of the organism. Our data has revealed the acceptable conditions for effective applications of ND and diamond materials.

4. Conclusions

In this study the biocompatibility of HTHP ND of size 100 nm is analyzed in terms of inducing immune response of macrophage (murine RAW 264.7 cell). Very low cytotoxicity for the macrophage was observed for 100 nm ND applied in concentrations up to 100 μ g/ml and no immune response was induced. ND doesn't provoke the expression of proinflammatory cytokines through mediating the nuclear translocation of certain transcriptional factors. Neither ND itself stimulates the immune response nor does

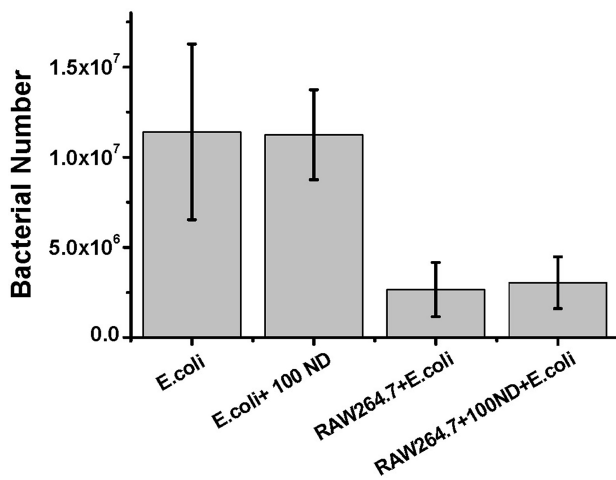


Figure 6 Effect of ND on antibacterial activity. *E. coli* colonies formation at treatment by RAW 264.7 and RAW 264.7 pre-incubated with 20 μ g/ml of 100 nm ND for 24 h. $n = 3$, ns, $P > 0.05$ was considered not significant. Data are mean \pm SD.

it interfere with macrophage's function, particularly in its antibacterial activity. Similarly to the uptake by other cells, ND was engulfed by macrophages via clathrin-dependent endocytosis pathway and is observed mainly encapsulated in the lysosome inside the cytoplasm. This can particularly explain the inertness of ND in interaction with the intercellular structures, as the limited side-effects provoked by ND in its bio applications, which gives the chance of ND as a biocompatible vehicle for drug delivery, etc. Thus, ND can be convenient platform for bio applications; however, proper conditions are extremely important. The understanding of the engulfment mechanism allows control the ND-containing complex (ND-based conjugate with drugs, etc.) tracing in the tissue, as well as the interaction with the macrophage and target cells.

Abbreviations

A549, human lung cancer cell line; ATP, Adenosine triphosphate; Beas 2b human bronchial epithelial cell; BSA – bovine serum albumin; FBS, fetal bovine serum; DAPI, 4',6-Diamidino-2-Phenylindole, Dihydrochloride; DIC, differential interference contrast; DMEM, Dulbecco's Modified Eagle's Medium; DMSO, dimethyl sulfoxide; DNA, Deoxyribonucleic acid; cDNA – complementary DNA; *E. coli*, bacteria Escherichia coli; EtBr, ethidium bromide; HFL-1 fibroblast-like human fetal lung cell; IRF-3, NF- κ B, AP-1, – transcriptional factors; I- κ B pre-complexed inhibitor of NF- κ B; LB, Luria-Bertani medium; LPS, lipopolysaccharides; M-MLV RT, Moloney Murine Leukemia Virus Reverse Transcriptase; MTT assay,

colorimetric assay for measuring the activity of cellular enzymes that reduce the tetrazolium dye, MTT; ND, nanodiamond; cND, carboxylated ND; DND, detonation ND, HTHP high temperature high pressure, NV, nitrogen vacancy; O.D.₆₂₀, optical density at 620 nm; PBS, phosphate buffer saline; Poly(I:C), Polyinosinic:polycytidyllic acid; RT-PCR, reverse transcription-polymerase chain reaction technique; RAW 264.7, the tissue-resident murine macrophages cell line; RAW-Blue cells are RAW 264.7 macrophages engineered with a secreted embryonic alkaline phosphatase (SEAP) gene; RNA, Ribonucleic acid; dsRNA, Double-stranded RNA; mRNA – Messenger RNA; TLR3, TLR4 – Toll-like receptors 3 and 4; TNF- α , IL-1 β , IL-6 IL-10 – proinflammatory cytokines.

Supporting Information

Additional supporting information may be found in the online version of this article at the publisher's website.

Author Contributions The manuscript was written through contributions of all authors. All authors have given approval to the final version of the manuscript. The authors contributed equally.

Acknowledgment The authors would like to thank the Ministry of Science and Technology (MoST) of Taiwan for financially supporting this project in a National Nano Science and Technology Program under grant MOST-102-2120-M259-001.

Author biographies Please see Supporting Information online.

References

- [1] J. Xie, S. Lee, and X. Chen, *Adv Drug Del Rev.* **62**, 1064–1079 (2010).
- [2] V. N. Mochalin, O. Shenderova, D. Ho, and Y. Gogotsi, *Nature Nanotechnol.* **7**, 11–23 (2012).
- [3] B. S. Zolnik, A. Gonzalez-Fernandez, N. Sadrieh, and M. A. Dobrovolskaia, *Endocrinology.* **151**, 458–465 (2010).
- [4] M. A. Dobrovolskaia, P. Aggarwal, J. B. Hall, and S. E. McNeil, *Mol Pharm.* **5**, 487–495 (2008).
- [5] R. Weissleder, M. Nahrendorf, and M. J. Pittet, *Nature Mater.* **13**, 125–138 (2014).
- [6] R. K. Tsai and D. E. Discher, *J Cell Biol.* **180**, 989–1003 (2008).
- [7] J. E. McDermott, M. Archuleta, B. D. Thrall, J. N. Adkins, and K. M. Waters, *PLoS ONE* **6**, e14673 (2011).
- [8] K. M. Waters, L. M. Masiello, R. C. Zangar, B. J. Taresevich, N. J. Karin, R. D. Quesenberry, S. Bandyopadhyay, *PLoS ONE* **6**, e14673 (2011).

- padhyay, J. G. Teeguarden, J. G. Pounds, and B. D. Thrall, *Toxicol Sci.* **107**, 553–569 (2009).
- [9] R. Klippstein, R. Fernandez-Montesinos, P. M. Castillo, A. P. Zaderenko, and D. V. Pozo, In-Tech Books, 309–324 (2010).
- [10] J. Park, D. H. Lim, H. J. Lim, T. Kwon, J. Choi, S. Jeong, and I.H. Choi, J. Cheon, *Chem Commun.* **47**, 4382–4384 (2011).
- [11] M. D. Massich, D. A. Giljohann, D. S. Seferos, L. E. Ludlow, C. M. Horvath, and C. A. Mirkin, *Mol Pharm.* **6**, 1934–1940 (2009).
- [12] O. Lunov, T. Syrovets, C. Loos, J. Beil, M. Delacher, K. Tron, G. U. Nienhaus, A. Musyanovych, V. Mai-länder, K. Landfester, and T. Simmet, *ACS Nano.* **5**, 1657–1669 (2011).
- [13] M. H. D. K. Al-Hallak, M. K. Sarfraz, S. Azarmi, M. H. G. Kohan, W. H. Roa, and R. Löbenberg, *The AAPS J.* **13**, 20–29 (2011).
- [14] C. H. Yeh, J. K. Hsiao, J. L. Wang, and F. Sheu, *J Nanopart Res.* **12**, 151–160 (2010).
- [15] K. K. Liu, C. L. Cheng, C. C. Chang, and J. I. Chao, *Nanotechnology.* **18**, 325102 (2007).
- [16] A. M. Schrand, H. Huang, C. Carlson, J. J. Schlager, E. Osawa, S. M. Hussain, S. M. Hussain, and L. Dai, *J Phys Chem B.* **111**, 2–7 (2007).
- [17] Y. Zhu, J. Li, W. Li, Y. Zhang, X. Yang, N. Chen, Y. Sun, Y. Zhao, C. Fan, and Q. Huang, *Theranostics.* **2**, 302–312 (2012).
- [18] Y. R. Chang, H. Y. Lee, K. Chen, C. C. Chang, D. S. Tsai, C. C. Fu, T. S. Lim, Y. K. Tzeng, C. Y. Fang, C. C. Han, H. C. Chang, and W. Fann, *Nat. Nanotech.* **3**, 284–288 (2008).
- [19] J. I. Chao, E. Perevedentseva, P. H. Chung, K. K. Liu, C. Y. Cheng, C. C. Chang, and C. L. Cheng, *Biophys J.* **93**, 2199–2208 (2007).
- [20] C. Y. Cheng, E. Perevedentseva, J. S. Tu, P. H. Chung, C. L. Cheng, K. K. Liu, J. I. Chao, P. H. Chen, and C. C. Chang, *Appl Phys Lett.* **90**, 163903 (2007).
- [21] K. K. Liu, C. C. Wang, C. L. Cheng, and J. I. Chao, *Biomaterials.* **30**, 4249–4259 (2009).
- [22] T. J. Wu, Y. K. Tzeng, W. W. Chang, C. A. Cheng, Y. Kuo, C. H. Chien, H. C. Chang, and J. Yu, *Nature Nanotechnol.* **8**, 682–689 (2013).
- [23] A. Krueger and D. Lang, *Adv Funct Mater.* **22**, 890–906 (2012).
- [24] V. N. Mochalin, A. Pentecost, X. M. Li, I. Neitzel, M. Nelson, C. Wei, T. He, F. Guo, and Yu. Gogotsi, *Mol. Pharmaceutics.* **10**, 3728–3735 (2013).
- [25] X. Q. Zhang, R. Lam, X. Xu, E. K. Chow, H. J. Kim, and D. Ho, *Adv Mater.* **23**, 4770–4775 (2011).
- [26] X. Q. Zhang, M. Chen, R. Lam, X. Xu, E. Osawa, and D. Ho, *ACS Nano.* **3**, 2609–2616 (2009).
- [27] Y. Li, Y. Tong, R. Cao, Z. Tian, B. Yang, P. Yang, *Int J Nanomedicine.* **9**, 1065–1082 (2014).
- [28] G. Xi, E. Robinson, B. Mania-Farnell, E. F. Vanin, K. W. Shim, T. Takao, E. V. Allender, C. S. Mayanil, M. B. Soares, D. Ho, and T. Tomita, *Nanomedicine.* **10**, 381–391 (2014).
- [29] L. Zhao, Y. H. Xu, T. Akasaka, S. Abe, N. Komatsu, F. Watari, and X. Chen, *Biomaterials.* **35**, 5393–5406 (2014).
- [30] M. A. Dobrovolskaia and S. E. McNeil, *Nature Nanotechnol.* **2**, 469–478 (2007).
- [31] O. Faklaris, D. Garrot, V. Joshi, F. Druon, J. P. Boudou, T. Sauvage, P. Georges, P. A. Curmi, and F. Treussart, *Small.* **4**, 2236–2239 (2008).
- [32] O. Faklaris, V. Joshi, T. Irinopoulou, P. Tauc, M. Sennour, H. Girard, C. Gesset, J. C. Arnault, A. Thorel, J. P. Boudou, P. A. Curmi, and F. Treussart, *ACS Nano.* **3**, 3955–3962 (2009).
- [33] A. Cuche, Y. Sonnefraud, O. Faklaris, D. Garrot, J. P. Boudou, T. Sauvage, J. F. Roch, F. Treussart, and S. Huant, *J Luminesc.* **129**, 1475–1477 (2009).
- [34] W. Busch, S. Bastian, U. Trahorsch, M. Iwe, D. Kühenel, T. Meißner, A. Springer, M. Gelinsky, V. Richter, C. Ikonomidou, A. Potthoff, I. Lehmann, and K. Schirmer, *J Nanopart Res.* **13**, 293–310 (2011).
- [35] E. Perevedentseva, S. F. Hung, K. J. Huang, I. T. Chiang, C. Y. Lee, Y. T. Tseng, C. L. Cheng, *J Nanopart Res.* **15**, 1834 (2013).
- [36] Y. Q. Li and X. P. Zhou, *Diam Relat Mater.* **19**, 1163–1167 (2010).
- [37] K. Solarska-Sciuk, A. Gajewska, S. Glinska, M. Studzian, S. Michlewska, Ł. Balcerzak, J. Skolimowski, B. Kolago, and G. Bartosza, *Chem Biol Interact.* **219**, 90–100 (2014).
- [38] A. P. Puzyr, A. V. Baron, K. V. Purtov, E. V. Bortnikov, N. N. Skobelev, O. A. Mogilnaya, and V. S. Bondar, *Diam Relat Mater.* **16**, 2124–2128 (2007).
- [39] A. P. Puzyr, D. A. Neshumayev, S. V. Tarskikh, G. V. Makarskaya, V. Yu. Dolmatov, and V. S. Bondar, *Diam Relat Mater.* **13**, 2020–2223 (2004).
- [40] H. Huang, E. Pierstorff, E. Osawa, and D. Ho, *ACS Nano.* **2**, 203–212 (2008).
- [41] O. A. Mogilnaya, A. P. Puzyr, A. V. Baron, and V. S. Bondar, *Nanoscale Res Lett.* **5**, 908–912 (2010).
- [42] T. Niemiec, M. Szmidt, E. Sawosz, M. Grodzik, and K. Mitura, *J Nanosci Nanotechnol.* **11**, 9072–9077 (2011).
- [43] A. Karpukhin, N. Avkhacheva, R. Yakovlev, I. Kulakova, V. Yashin, G. Lisichkin, and V. G. Safranova, *Cell Biol Int.* **36**, 727–733 (2011).
- [44] V. Thomas, B. A. Halloran, N. Ambalavanan, S. A. Catledge, and Y. K. Vohra, *Acta Biomater.* **8**, 1939–1947 (2012).
- [45] N. Mohan, C. S. Chen, H. H. Hsieh, Y. C. Wu, and H. C. Chang, *Nano Lett.* **10**, 3692–3699 (2010).
- [46] P. H. Chung, E. Perevedentseva, J. S. Tu, C. C. Chang, and C. L. Cheng, *Diam Relat Mater.* **15**, 622–626 (2006).
- [47] S. Copeland, H. S. Warren, S. F. Lowry, S. E. Calvano, and D. Remick, *Clin Diagn Lab Immunol.* **12**, 60–67 (2005).
- [48] S. Akira, S. Uematsu, and O. Takeuchi, *Cell.* **124**, 783–801 (2006).
- [49] E. Perevedentseva, C. Y. Cheng, P. H. Chung, J. S. Tu, Y. H. Hsieh, and C. L. Cheng, *Nanotechnology.* **18**, 315102 (2007).
- [50] C. Hanley, A. Thurber, C. Hanna, A. Punnoose, J. Zhang, and D. G. Wingett, *Nanoscale Res Lett.* **4**, 1409–1420 (2009).
- [51] S. Kim, W. K. Oh, Y. S. Jeong, J. Y. Hong, B. R. Cho, J. S. Hahn, and J. Jang, *Biomaterials.* **32**, 2342–2350 (2011).

- [52] L. Müller, M. Riediker, P. Wick, M. Mohr, P. Gehr, and B. Rothen-Rutishauser, *J R Soc Interface*. **7**, S27–S40 (2010).
- [53] P. G. Barlow, A. Clouter-Baker, K. Donaldson, J. MacCallum, V. Stone, *Part Fibre Toxicol.* **2**, 11 (2005).
- [54] X. Banquy, F. Suarez, A. Argaw, J. M. Rabanel, P. Grutter, J. F. Bouchard, P. Hildgen, and S. Giasson, *Soft Matter*. **5**, 3984–3991 (2009).
- [55] A. S. Zahr, C. A. Davis, and M. V. Pishko, *Langmuir* **22**, 8178–8185 (2006).
- [56] N. Gao, Q. Zhang, Q. Mu, Y. Bai, L. Li, H. Zhou, E. R. Butch, T. B. Powell, S. E. Snyder, G. Jiang, and B. Yan, *ACS Nano*. **5**, 4581–4591 (2011).
- [57] C. Villiers, H. Freitas, R. Couderc, M. B. Villiers, and P. Marche, *J Nanopart Res.* **12**, 55–60 (2010).